Computers in Biology and Medicine 41 (2011) 716–725

Contents lists available at ScienceDirect

Computers in Biology and Medicine

journal homepage: www.elsevier.com/locate/cbm

Automatic brain extraction methods for *T*1 magnetic resonance images using region labeling and morphological operations

K. Somasundaram *, T. Kalaiselvi

Department of Computer Science and Applications, Gandhigram Rural Institute, Gandhigram, Tamilnadu 624302, India

ARTICLE INFO

Article history:
Received 4 February 2010
Accepted 14 June 2011

Keywords:
Brain extraction
Intensity thresholding
Labeling
Region identification
Segmentation
Abnormal MRI head scans

ABSTRACT

In this work we propose two brain extraction methods (BEM) that solely depend on the brain anatomy and its intensity characteristics. Our methods are simple, unsupervised and knowledge based. Using an adaptive intensity thresholding method on the magnetic resonance images of head scans, a binary image is obtained. The binary image is labeled using the anatomical facts that the scalp is the boundary between head and background, and the skull is the boundary separating brain and scalp. A run length scheme is applied on the labeled image to get a rough brain mask. Morphological operations are then performed to obtain the fine brain on the assumption that brain is the largest connected component (LCC). But the LCC concept failed to work on some slices where brain is composed of more than one connected component. To solve this problem a 3-D approach is introduced in the BEM. Experimental results on 61 sets of *T*1 scans taken from MRI scan center and neuroimage web services showed that our methods give better results than the popular methods, FSL's Brain Extraction Tool (BET), BrainSuite's Brain Surface Extractor (BSE) gives results comparable to that of Model-based Level Sets (MLS) and works well even where MLS failed. The average Dice similarity index computed using the "Gold standard" and the specificity values are 0.938 and 0.992, respectively, which are higher than that for BET, BSE and MLS. The average processing time by one of our methods is ≈ 1 s/slice, which is smaller than for MLS, which is ≈ 4 s/slice. One of our methods produces the lowest false positive rate of 0.075, which is smaller than that for BSE, BET and MLS. It is independent of imaging orientation and works well for slices with abnormal features like tumor and lesion in which the existing methods fail in certain cases.

1. Introduction

Magnetic Resonance Imaging (MRI) is one of the non-destructive, non-intrusive methods and a safe modality for medical diagnosis. The most important advantage of the MRI is its ability to provide good contrast between various organs and tissues and the three-dimensional nature of imaging methods [1]. With its dependence on the more biologically variable parameters, proton density (*PD*), longitudinal relaxation time (*T*1) and transverse relaxation time (*T*2) variable image contrast can be achieved using different pulse sequences and changing the imaging parameters. Three types of images, *PD*, *T*1 and *T*2, are produced and their signal intensities relate to specific tissue characteristics. In each type, images are taken in any one of the three orientations: axial (neck to head), coronal (front to back) and sagital (ear to ear).

The removal of non-brain regions like scalp, skull (bone), fat, eyes, neck, etc., from MRI of head scans is an important area of study as it helps to improve the speed and accuracy of diagnostic and prognostic procedures in medical applications [2]. This procedure is often referred as Brain-Extraction/Skull-Stripping. Segmentation of brain region from MRI of head scans plays a vital role in coregistration, multimodality registration, brain tissue segmentation, pathologies detection, cortical surface modeling and visualization techniques. Numerous brain extraction tools were developed and tested on a variety of datasets. But they are limited to specific orientation or the type or datasets and forced the user to compromise either on the processing speed or the accuracy. Some of the brain extraction algorithms (BEA) for extracting brain from single echo *T*1 images are Statistical Parameter Mapping v.2 (SPM2) [3], FSL's Brain Extraction Tool (BET) [4], BrainSuite's Brain Surface Extractor (BSE) [5,6], AFNI's 3dIntracranial [7], FreeSurfer's MRI Watershed [8], Model-based Level Sets (MLS) [9], Exbrain [10] and the Simon Fraser University (SFU) method [11]. Recently Somasundaram and Kalaiselvi developed a BEA for *T*1 images [12] and *T*2 images [13].

Several studies [3,14–18] compared the performance of the most commonly used BEAs and concluded that the existing algorithms had both strengths and weaknesses. Some of the existing hybrid methods are Minneapolis Consensus Strip (MCS) [17], Brain Extraction Meta Algorithm (BEMA) [18] and Hybrid Watershed Algorithm (HWA) [19]. MCS outperforms other methods but the tool dependency and setup procedure are too complex for practical use [20].

* Corresponding author. Tel.: +91 451 2452371; fax: +91 451 2453071.
E-mail addresses: somasundaramk@yahoo.com (K. Somasundaram), kalai_tvp@yahoo.co.in (T. Kalaiselvi).

0010-4825/$ - see front matter © 2011 Elsevier Ltd. All rights reserved.
doi:10.1016/j.compbiomed.2011.06.008

Thus no single algorithm appears to have produced accurate results without initialization and computational complexity. Ravinda and Jagath [21] suggested that a fully automated procedure to extract the brain from a large database of *T*1 MRI of head scans must have the capability to extract the brain accurately from all the images without any human intervention during the peeling process. Further, the procedure should not require any preprocess of the images outside the chain of image processing routines. Our present study follows this lead given by Ravinda and Jagath [21] and sets our goal to develop an automatic tool to extract the brain portion from *T*1 head scans.

The proposed methods are simple, unsupervised and knowledge based approaches. The main head features like scalp, skull and brain and their MRI intensity characteristics are used in our approach. In most of the *T*1 scans, skull is a dark portion and lies between the two brighter regions, scalp and brain. Using this expert knowledge either the scalp is removed or the brain is extracted to get a rough brain portion. The generation of coarse brain portion is purely a nonparametric and unsupervised process. Run length identification (RLI) scheme is used for region labeling and searching. Then a set of segmentation processes such as morphological operations and connected component analysis (CCA) are done to produce a fine brain. This segmentation stage is adaptable to any of the existing methods and extendable to 3-D schemes. Application of our algorithms on standard real image datasets show that the proposed methods work better than the popular algorithms BET, BSE and MLS.

The remaining part of the paper is organized as follows. In Section 2, we present the methods that we have developed to extract brain. The materials used for our study are given in Section 3 and the experimental results and discussions are given in Section 4. Finally we conclude the paper in Section 5.

2. Methods

In this work we propose two fully automatic, two-stage brain extraction methods (BEM) to extract the brain portion from *T*1 MRI of head scans. In Stage-1, the feature extraction is done to locate the region of interest (ROI) and in Stage-2, segmentation is done to extract the ROI. In our work, the ROI is the brain region. Region labeling plays a major role in Stage-1 for detecting the brain area and to produce the rough brain portion. Morphological operations are used in Stage-2 to segment the fine brain portion.

2.1. Stage-1: feature extraction

The objective of the Stage-1 is to obtain a rough brain portion. The features found in the brain are used for this process. For feature extraction an expert knowledge that solely depends on the brain anatomy and intensity characteristics of *T*1 scans is used. In *T*1 MRI of head scans, scalp and brain tissues are brighter than CSF, skull and background [10]. Skull is the boundary separating brain and scalp.

Using the above expert knowledge, either the bright scalp is detected and removed from the slice or the bright brain is identified and retained in the slice. Thus the main feature we try to identify from the image is either the scalp or the brain. The scalp removal technique is named as scalp removal process (SRP) and the brain extraction technique is called as brain extraction process (BEP). We use either of these processes to produce the rough brain portion in this stage. The flowchart for Stage-1 is shown in Fig. 1. The images corresponding to input, output and the intermediate processes are given alongside of the flowchart in Fig. 1.

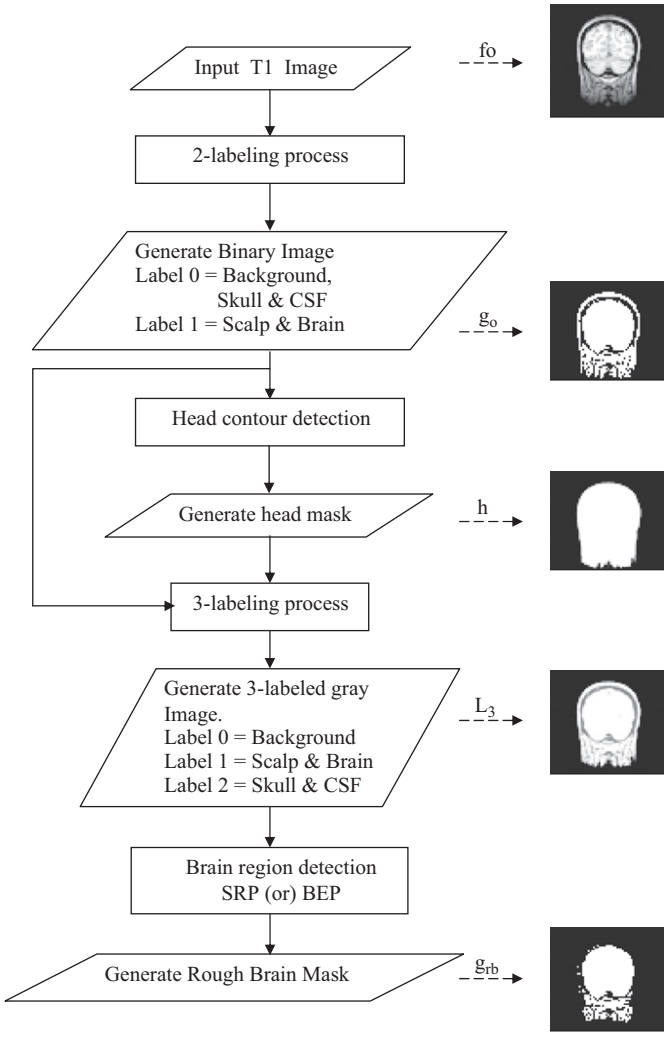

Fig. 1. Flowchart of Stage-1: feature extraction.

2.1.1. Thresholding and 2-labeling process

Stage-1 starts with the 2-labeling process for the given input *T*1 image. Initially, an optimal intensity threshold value (T_{opt}) for the pixels of the input *T*1 image (f_0) is calculated using Ridler's method [22]. This algorithm is iterative, four to ten iterations usually being sufficient [22]. At iteration t, the threshold value T_{t+1} is computed as follows:

$$T_{t+1} = \frac{\mu_{bgt} + \mu_{obt}}{2} \tag{1}$$

where μ_{bgt} and μ_{obt} are the mean background (bg) and object (ob) gray-level at iteration t, respectively. The segmentation into background and object at step t is defined by the threshold value T_t determined in the previous iteration. The threshold value computed at 10th iteration is considered as optimal threshold value T_{opt} and it is used to identify and separate objects from the surrounding uniform background [22]. A binary image $g_0(x, y)$ is obtained using T_{opt} as

$$g_0(x,y) = \begin{cases} 1 & \text{if } f_0(x,y) \geq T_{opt} \\ 0 & \text{otherwise} \end{cases} \tag{2}$$

where, $f_0(x, y)$ is the original intensity of the image at pixel (x, y). Thus the binary image g_0 has two labels: label 0 to dark regions like background, skull and csf, and label 1 to bright regions like scalp and brain as shown in Fig. 1. The image g_0 contains few contour like regions. The outermost dark region is the

background, the next white region represents the scalp, the inner dark region represents the skull and CSF and the innermost white region represents the brain.

2.1.2. Head contour detection

Next we proceed to detect the boundary separating the scalp and the background to produce the head mask. For this, we traverse the binary image g_0 from the four sides, pixel by pixel, starting from the left side followed by right, top and bottom and trace towards the opposite side to detect the border of the head. The scalp is a bright region in $T1$ images. Hence the 0–1 (black to white) transition during the traversal in g_0 is marked as the head border point $b(x, y)$, for all rows and columns of the image. Then a region R_h is formed which is bounded by a set of $b(x, y)$ found earlier. This region is considered as head and the rest is treated as background. Finally, an image h representing the head mask is obtained as

$$h(x,y) = \begin{cases} 1 & \text{if } (x,y) \in R_h \\ 0 & \text{otherwise} \end{cases} \quad (3)$$

In the image h, shown in Fig. 1, the region containing value 1's (white) is the R_h representing head and the region containing values 0's (black) is the background (R_{bg}). The two regions then satify

$$h = R_h \cup R_{bg} \quad (4)$$

2.1.3. 3-Labeling process

Next, we proceed to identify the inner dark region representing the skull and the CSF. This is done by marking that region with label 2. For this operation, we take the binary image g_0 and take R_h as the region of interest. Within R_h, we select the pixels corresponding to dark portions representing skull and/or CSF using the binary image g_0 and mark them with a label 2. Already g_0 is a two-labeled image with values 0 and 1. With the new label 2, the whole image becomes a 3-labeled image and is denoted as L_3. The labeling is done as follows:

$$L_3(x,y) = \begin{cases} 2 & \text{if } g_0(x,y) = 0 \text{ and } (x,y) \in R_h \\ 1 & \text{if } g_0(x,y) = 1 \\ 0 & \text{if } g_0(x,y) = 0 \end{cases} \quad (5)$$

Now we have L_3, a 3-labeled image, with pixels in the background labeled as 0, the pixels in the regions of scalp and brain tissues labeled as 1 and the remaining pixels representing skull, CSF, etc., labeled as 2. The resultant L_3 is shown in Fig. 1. Label 0 is dark, 1 is white and 2 is gray. Each labeled region is given some gray shades for display purpose.

2.1.4. Brain region detection

We then proceed to extract the rough brain portion. For this, we employ SRP or BEP. The SRP and BEP are based on run length identification scheme for labeling [21]. First, we construct horizontal runs for regions with label 1 of L_3 that corresponds to scalp and brain regions. Next, we check the label values of pixels that are connected horizontally to each run and classify them into two cases I and II. The classification of the runs is done based on the edges of that run. The runs between background (0) to background (0), background (0) to skull (2), and skull (2) to background (0) are classified as case I. The runs between skull/CSF (2) to skull/CSF (2) are classified as case II. Here the numbers within the parenthesis 0 and 2 represent the label of the pixel.

2.1.5. Scalp removal process (SRP)

If a run satisfies case I then these runs are marked as R_{sc} (scalp).The intensity of the pixels belonging to R_{sc} are set to 0 and the rest is retained as such in g_0 to produce a rough brain mask g_{rb} and is given by

$$g_{rb}(x,y) = \begin{cases} 0 & \text{if } (x,y) \in R_{sc} \\ g_0(x,y) & \text{otherwise} \end{cases} \quad (6)$$

By this process the bright scalp is merged with the background.

2.1.6. Brain extraction process (BEP)

If a run satisfies case II then these runs are marked as R_{bt} (brain tissue). The pixels corresponding to these runs are retained in g_0 and the intensities of other pixels are set to background value 0 and the rough brain mask g_{rb} is obtained as

$$g_{rb}(x,y) = \begin{cases} g_0(x,y) & \text{if } (x,y) \in R_{bt} \\ 0 & \text{otherwise} \end{cases} \quad (7)$$

Using either of these processes (SRP or BEP), Stage-1 produces a rough brain mask as shown in Fig. 1. Both SRP and BEP produce the same result. If the original image f_0 is used instead of binary form g_0 in Eqs. (6) and (7) then the rough brain portions f_{rb} will be produced as shown in Fig. 2(a) and (b).

2.2. Stage-2: segmentation

The aim of the segmentation stage is to produce a fine brain mask from the rough brain mask g_{rb}, produced in Stage-1. Image processing techniques, morphological operations and connected component operation are performed in this stage. The sequence of these processes is given in Fig. 3.

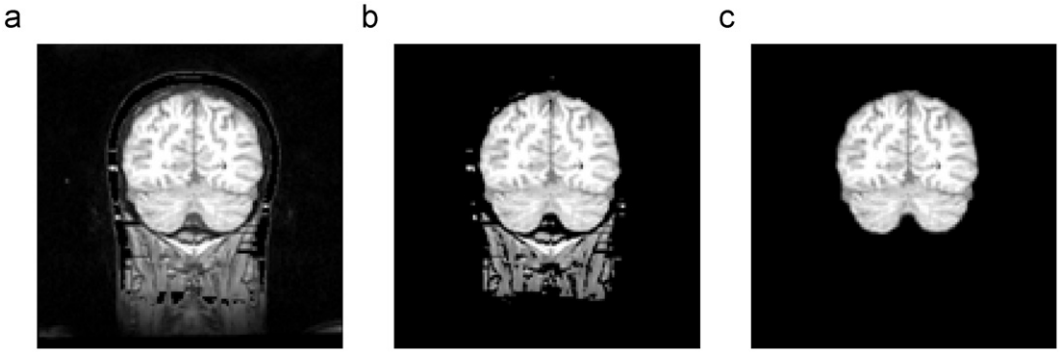

Fig. 2. (a) Rough brain portion f_{rb} produced by SRP in Stage-1 using the original image f_0; (b) rough brain portion f_{rb} produced by BEP in Stage-1 using the original image f_0; and (c) final brain portion f_{fb} produced by segmentation process in Stage-2 using the final mask X_3 and original image f_0.

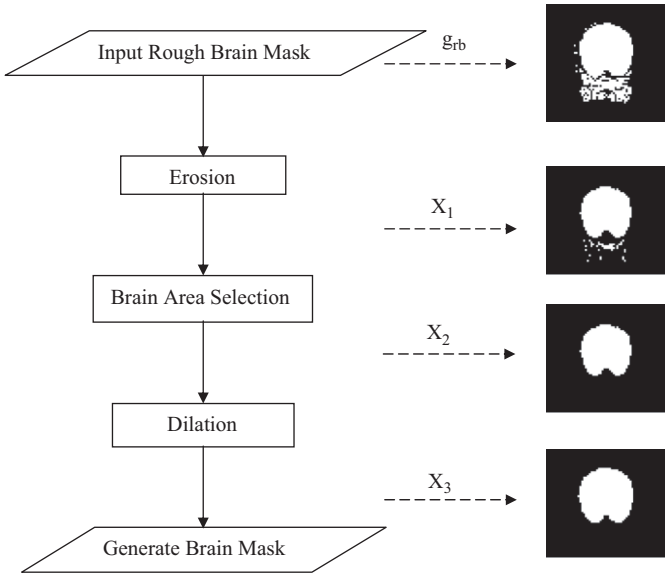

Fig. 3. Flowchart of Stage-2: segmentation.

2.2.1. Binary erosion

The binary image g_{rb} obtained in Stage-1 is eroded by an octagonal structuring element with a 7×7 size (O_7) to get an eroded image X_1. The binary erosion is used to separate the weakly connected regions. After the erosion, the binary image X_1 will have several disconnected regions as shown in Fig. 3. Let there be n regions ($R(i)$, $i=1,\ldots,n$) in the eroded image X_1. The area $R_A(i)$ of the ith region $R(i)$ is the total number of pixels in that region and is computed using the run length identification scheme.

2.2.2. Brain region selection

The next step is to select the brain region. Let R_{fb} be the region of final brain. Initially it is set to null:

$$R_{fb} = \varphi \tag{8}$$

The area of each connected regions $R_A(i)$ is calculated. For each slice, the largest connected component (LCC) among the regions obtained in the eroded image is treated as the brain portion R_{fb}. The brain selection is done as follows:

$$R_{LCC} = R\left(\arg\max_{1 \le i \le n} R_A(i)\right) \tag{9}$$

$$R_{fb} = R_{LCC} \tag{10}$$

After identifying the brain portion R_{fb} in the binary image X_1, we extract the brain region X_2 as

$$X_2(x,y) = \begin{cases} 1 & \text{if } (x,y) \in R_{fb} \\ 0 & \text{otherwise} \end{cases} \tag{11}$$

The brain region X_2 extracted by applying Eqs. (9)–(11) is shown in Fig. 3.

2.2.3. Binary dilation

To recover the pixels that were lost due to thresholding and erosion, the dilation operation is performed on X_2 using the same structuring element O_7 at the border to get a dilated image. The dilated binary image X_3 is taken as the brain mask and a sample is shown in Fig. 3. Using X_3, the final brain portion (f_{fb}) is extracted from the original MR scan (f_0) and is given by

$$f_{fb}(x,y) = \begin{cases} f_0(x,y) & \text{if } X_3(x,y) = 1 \\ 0 & \text{otherwise} \end{cases} \tag{12}$$

The final brain portion extracted by our method is shown in Fig. 2(c). This is purely a two-dimensional approach to extract the brain and is named as BEM2D.

2.3. BEM2DE

The selection of a region on the basis of LCC as brain by Eq. (10) gives, in few cases, either a partial brain or a non-brain region as shown in column 2 of Fig. 4 for the original images given at column 1. In some brain volumes few slices might contain more than one connected component and yet correspond to brain. Such volumes are

i. At the posterior and anterior ends of coronal volume, where the cerebral hemispheres appear as two regions.
ii. Upper slices near the top of head of axial volume, where the cerebral hemispheres appear as two regions.
iii. In the very lower portions of axial volume, in which the temporal and frontal lobes are separated from the cerebellum.
iv. In the middle slices, narrow openings either in head or skull due to partial volume effect (PVE) that splits the brain into two or more regions.

In order to obtain the complete brain portion and to discard the non-brain region, we make use of 3-D information available in adjacent slices of that volume. This extended method is named as BEM2DE. In MRI of head scans, there is a continuity of the brain portion between two adjacent slices. This similarity property, in addition to overlap test procedure, is used to select the proper brain regions as discussed in [13]. Jaccard coefficient (J) [23] is used to estimate the similarity between the brain mask of the current slice and the previous slice. If J is greater than 85% the segmented result is considered as brain portions, otherwise an overlap ratio (V) of each region (R) with the brains mask of the previous slice (P) is computed using

$$V(P,R)_i \frac{N(R \cap P)}{N(R)} \tag{13}$$

For an anisotropic nature of volume, V is expected to be more than 90%. But the narrow openings through the weak boundaries of head or skull may split or reduce the size of the region that is present with P. We set $V=70\%$ in our method. The values 85% and 70% for J and V, respectively, were estimated after doing several trial experiments. For any ith region $R(i)$, if $V_i > 70\%$ then the region $R(i)$ is treated as a brain portion, and is added to the brain region R_{fb}, otherwise it will be discarded. Hence for the eroded brain X_1, with more than one connected components, Eq. (10) is modified as

$$R_{fb} = \begin{cases} R_{fb} \cup_{1 \le i \le n} R(i) & \text{if } V_i > 70\% \\ R_{fb} & \text{otherwise} \end{cases} \tag{14}$$

In MRI of head scans, the middle slices contain only one connected region. Therefore, identifying the brain portion is simple and easy. Therefore, in the BEM2DE method we start with the center slice for each brain volume, at approximately $W/2$th position, where W is the total number of slices in the volume and proceed in each direction, up and down, to obtain the result. Finally a binary image (X_2) of the selected brain region (R_{fb}) is created using Eq. (11) and used to extract the fine brain portion.

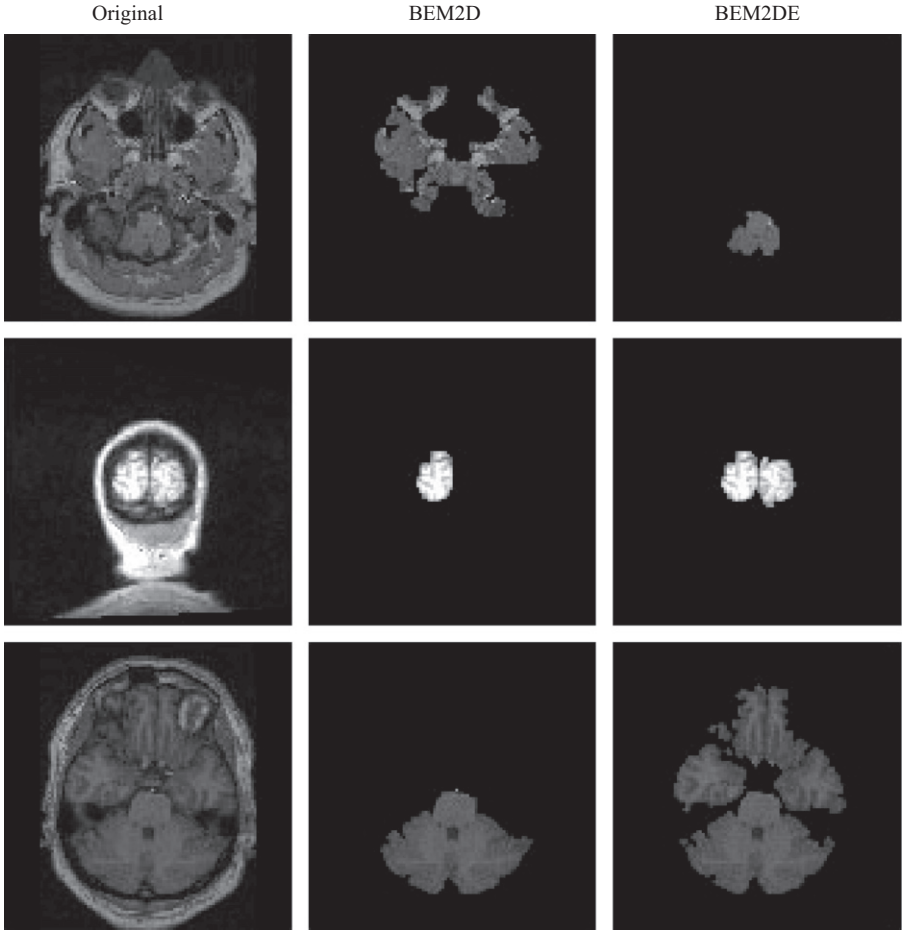

Fig. 4. Original images from different orientations are given in column 1. The results of BEM2D are in column 2 and the results of BEM2DE are in column 3.

2.4. Evaluation parameters

For evaluating the performance of our methods we make use of Dice coefficient, sensitivity, specificity, false positive rate and false negative rate. Several popular quantitative measures are available for comparing structural similarities of two images. Dice coefficient and Jaccard's coefficient (measure of similarity) are such measurements of asymmetry information on binary (and non-binary) variables. The Dice coefficient (D) [24] is given by

$$D(A,B) = \frac{2|A \cap B|}{|A| + |B|} \tag{15}$$

where A and B are two datasets. The value D varies from 0 for complete disagreement to 1 for complete agreement, between A and B.

The sensitivity (S) is the percentage of brain voxels recognized by the algorithm and specificity (Sp) is the percentage of non-brain voxels recognized by the algorithm and are computed using the true positive (TP), false positive (FP), true negative (TN) and false negative (FN) values of the brain extracted by an algorithm. TP and FP are the total number of pixels correctly and incorrectly classified as brain tissue by the automated algorithm. TN and FN are defined as the total pixels correctly and incorrectly classified as non-brain tissue by the automated algorithm:

$$S = \frac{TP}{TP + FN} \tag{16}$$

$$Sp = \frac{TN}{TN + FP} \tag{17}$$

Finally, false positive rate (FPR) and false negative rate (FNR) are used to measure the misclassification done by the algorithm. FPR is the number of voxels incorrectly classified as brain tissue by the automated algorithm divided by manually segmented brain masks and is given by

$$FPR = \frac{FP}{TP + FN} \tag{18}$$

FNR is the number of voxels incorrectly classified as non-brain tissue by the automated algorithm divided by manually segmented brain masks and is given by

$$FNR = \frac{FN}{TP + FN} \tag{19}$$

The FPR represents the degree of under segmentation and the FNR the degree of over segmentation.

3. Materials

We used 61 $T1$ datasets obtained from the following sources for our experiments.

Twenty coronal datasets of normal subjects were obtained from the Internet Brain Segmentation Repository (IBSR) developed by Centre for Morphometric Analysis (CMA) at Massachusetts General Hospital. Each set has approximately 60 slices with slice thickness ≈ 3 mm and matrix $= 256 \times 256$. Some datasets were affected by intensity non-uniformity (INU) artifact caused by magnetic fields, radio frequency coils and noise factors. The presence of neck portion along with head was much higher in some datasets and had intensities similar to brain tissues.

Table 1
MRI *T*1 datasets collected from 'The Whole Brain Atlas'.

Dataset	Gender	Age	Clinical	Total slices
1	Male	73	Glioma—II Grade Astrocytoma	124
2	Male	22	Sarcome	24
3	Female	36	Cerebral calcinosis	18
4	Male	30	Multiple sclerosis	24
5	Male	31	Cerebral toxoplasmosis	24
6	Female	49	Multiple embolic infarction	24
7	Male	51	Multiple embolic infarctions	24
8	Female	49	Cerebral hemorrhage	24
9	Male	70	Mild Alzheimer's diseases	24
10	Female	71	AD-visual hallucination	55
11	Female	59	Pick's diseases	23
12	Female	76	Vascular dementia	43
13	Female	71	Fatal stroke	24
14	Male	76	Chronic subdural hematoma	26

The manually segmented masks, ground truth or gold standard, are also provided by the CMA.

Twelve datasets of MRI of Head Scans were collected from KGS Advanced MR and CT Scans, Madurai, Tamilnadu, India. The MRI datasets were acquired on a Siemens 1.5T scanner and each dataset contained nearly 20 slices.

Another fifteen *T*1 test datasets were obtained from Brain Extraction Evaluation (BEE) web service maintained by the International Neuroimaging Consortium (INC), University of Minnesota. Some of the datasets were affected either by wrap around artifact or by zipper artifact.

Fourteen *T*1 abnormal datasets are taken from 'The Whole Brain Atlas' (WBA) website maintained by the Department of Radiology and Neurology at Brigham and Women's Hospital, Harvard Medical School, the Library of Medicine, and the American Academy of Neurology. The details of datasets are given in Table 1. These were used to evaluate our methods on datasets with abnormalities.

4. Results and discussions

We carried out experiments by applying our BEM2D and BEM2DE on 61 datasets of *T*1 images of the head scans and performed quantitative and qualitative analysis on the extracted brain portion. To estimate the performance of our methods, we compared our results with the well-known brain extractors BET, BSE and MLS. Manual segmentation masks were unavailable for the images collected from BEE web service, KGS scan centre and WBA website. Therefore they were evaluated qualitatively. We used BET, MRIcro 1.40, with a default smoothness value of 0.50. For BSE we used BrainSuite 2.0 with the default values 3, 5, 0.75 and 1 for the number of iterations, diffusion constant, edge constant and erosion size, respectively. Since BSE is an interactive tool the values should be adjusted to yield good segmentation results for some volumes. The MLS software was obtained from the software collections maintained by Laboratory of Neuro Imaging (LONI), University of California at Los Angeles (UCLA) and used with the default values specified by the software.

4.1. Quantitative evaluation

For a quantitative comparison of the performance of our methods with BET, BSE and MLS, the "gold standard", manually extracted brain from *T*1 weighted MRI brain datasets available at IBSR website, was used. For quantitative analysis, the parameters *D*, *S*, *Sp*, *FPR*** and *FNR* were computed using Eqs. (15)–(19).

First we carried out experiments on the 20 datasets available in IBSR. Fig. 5 shows the plot of average Dice coefficient for the 20 datasets. The labels along *x*-axis are the names of the IBSR datasets. The average value of Dice coefficient, *D*, of BET is very low for the datasets 1_24, 5_8, 6_10, 7_8, 8_4, 15_3, 16_3 and 17_3. The reason is either due to INU artifact among the datasets or the inability to remove neck portion. The *D* value obtained by BSE was lower for datasets 5_8, 6_10, 15_3 and 17_3 due to the intensity variation among the slices. Adjustments of parameters (3, 25, 0.62, 1) were done in BrainSuite 2.0 for the datasets 5_8, 6_10 and 15_3 so as to get the best result. BSE produced higher values of *D* for the datasets 110_3, 111_2 and 205_3 than the proposed methods. But the deviation of *D* value among the datasets, as shown in Fig. 5, is higher for BSE and BET than the proposed and MLS methods. MLS and BEM2DE are found to give the highest similarity coefficient for all the datasets. But for the dataset 6_10, MLS selected the neck portions from the coronal scans instead of brain and hence failed to produce the result. Hence the best and consistent performance, irrespective of INU artifact, image contrast and involvement of excess portions like neck, eyes and other non-brain tissues, is attained by the proposed methods.

The quantitative values obtained for the *D*, *S*, and *Sp* using our methods for the 20 datasets of IBSR are given in Table 2. To evaluate the performance of our methods, the results obtained for BET, BSE and MLS are also given. From Table 2, we note that the highest value for *D*, 0.938, is obtained by our method BEM2DE, the best value for sensitivity *S*, 0.998, by BET, and the best value for specificity *Sp*, 0.992, by the proposed methods. From Fig. 5 we note that our methods give better consistencies with low standard deviation.

The computed values for the parameters *FPR* and *FNR* and total misclassification rate are given in Table 3. The *FPR* of BET is greater than that of other methods and indicates that it has included more

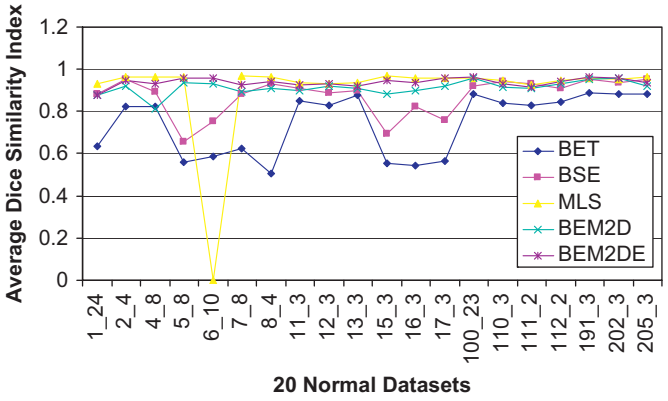

Fig. 5. The Dice coefficient (similarity measure) obtained for existing BEAs (BET, BSE and MLS) and proposed BEMs (BEM2D and BEM2DE) on each of the 20 normal datasets from the IBSR. The labels at the *x*-axis are the datasets names given in IBSR.

Table 2
Mean value and standard deviation for the parameters Dice coefficient, sensitivity and specificity calculated on 20 normal datasets taken from the IBSR. The best performance for each metric is highlighted.

Method	Similarity measure Dice (*D*)	Sensitivity (*S*)	Specificity (*Sp*)
BET	0.741 ± 0.146	$\mathbf{0.998 \pm 0.002}$	0.915 ± 0.055
BSE	0.874 ± 0.088	0.885 ± 0.116	0.99 ± 0.012
MLS	0.905 ± 0.213	0.936 ± 0.22	0.987 ± 0.017
BEM2D	0.913 ± 0.033	0.909 ± 0.063	$\mathbf{0.992 \pm 0.006}$
BEM2DE	$\mathbf{0.938 \pm 0.021}$	0.951 ± 0.036	$\mathbf{0.992 \pm 0.006}$

Table 3
Average value of *FPR*, *FNR* and total misclassification rate for 20 datasets taken from IBSR.

Method	*FPR*	*FNR*	Total misclassification rate (*FPR*+*FNR*)
BET	0.878	0.003	0.881
BSE	0.086	0.115	0.201
MLS	0.119	0.064	0.183
BEM2D	0.066	0.091	0.157
BEM2DE	0.075	0.049	0.124

non-brain tissues than other methods. *FNR* of BSE is high and implies that it has excluded several brain tissues from the final result than other methods. For a better performance the sum of *FPR* and *FNR*, i.e., the total misclassification rate should be as low as possible. Our method BEM2DE gives the lowest value implying that it is the best BEA with lower errors than BET, BSE and MLS.

The experiments were performed in a 1.73 GHz Intel Pentium dual-core processor, Windows XP with 1 GB RAM using Matlab 6.5. The average processing times of the proposed BEM2D and BEM2DE methods on IBSR datasets were approximately 0.7 and 1 s/slice, respectively. BET and BSE took less than 0.5 s/slice to produce the final result but the excess *FPR* with BET and *FNR* with BSE are unavoidable. This shows that the manual intervention is required to redefine the final result. MLS took ≈ 4 s/slice and even consumed longer time to real datasets.

4.2. Qualitative evaluation

Then we applied our methods, BET, BSE and MLS on the second set of 15 datasets of BEE service. Slices 16, 26, 36, 46, 56, 66, 76, 86, 96, 116, 126 and 136 were selected at regular intervals from subject01 of BEE web service. The brain portions extracted by the existing and proposed methods are given in Figs. 6 and 7. Under segmentation is experienced by BET in slices 46, 56 and 66 (row 2). BSE (row 3) was unable to produce any result for first two slices (16 and 26) and over-extraction was done in slices 36–106. The proposed BEM2D failed to extract the correct brain as seen in slices 16, 26,36, 46 and 56. Our BEM2DE and MLS produced acceptable results for all the slices.

We then carried out experiments on the third set containing 12 real image datasets obtained from the KGS Scan Centre. Samples of the brain extracted by each method for different orientations are given in Fig. 8. The original slices selected from axial (slice 1 and slice 2), coronal (slice 3 and slice 4) and sagittal (slice 5 and slice 6) orientations of a normal subject are given in first row of Fig. 8. The results obtained by each method are given in successive rows. From Fig. 8 we note that the results obtained by our methods are better than the results obtained from the well-known methods BET, BSE and MLS. BET includes some additional non-brain tissues along with the brain tissues and requires some post-processing operations to remove the extra tissues (see the BET results of slices 1, 5 and 6 in row 2 of Fig. 8). Over-extraction is done by BSE and it removes some brain tissues along the cerebral border and inside the brain as shown in row 3 of Fig. 8 for slices 1 through 6.

BET smoothens the image for low contrast images and thus enhances and extracts the brain region from original images as shown in row 2 (slices 1 and 2) of Fig. 8. But this is not possible for all situations. When the same principle is applied for extremely poor contrast images, BET failed to extract the brain region (slices 3 and 4). Further, when we applied BSE on the datasets it was unable to extract the brain region for the entire dataset even after setting different values to model parameters. From the results of BET and BSE for slices 3 and 4 given in Fig. 8, it can be seen that BET and BSE failed to work on extremely poor contrast images. MLS worked on axial and coronal volumes whereas it failed to extract the brain region from sagittal scans (slices 5 and 6 in row 6). MLS also included some additional non-brain tissues with the final result (slices 1, 3 and 4). Our BEM2D produced partial brain portions (slice 3 in row 4 of Fig. 8) whereas the BEM2DE extracted them correctly.

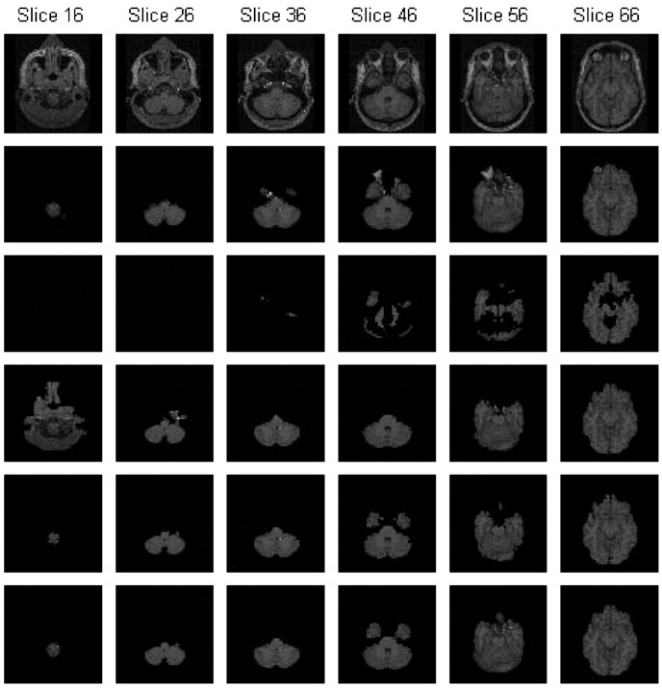

Fig. 6. Brain portion extracted using the existing and proposed algorithms on *T*1 head scans selected from the lower portions of axial volume of BEE web service. Row 1 shows original *T*1 scans and rows 2–6 show brain portion extracted by BET, BSE, BEM2D, BEM2DE and MLS, respectively.

The WBA contains MRI of head scans of patients with different brain abnormalities. None of the BEAs, BSE, BET and MLS worked successfully on these images. To test the robustness of our method, we applied our BEM2DE on the 14 datasets given in Table 1. BEM2DE worked well for the first 8 sets and the results of the initial slices are given in Fig. 9. The selection of initial slice is an important factor to start our method. If the brain portion in the initial slice could not be extracted properly, then our method fails. It is a drawback of our method. This happened for the dataset 9, which had the image of Alzheimer's disease. In this, the middle slice (slice 12) had brain tissue discontinuity along the mid-sagital line. As a result only half of the brain was extracted and therefore, the extraction done in the remaining slices keeping that as a reference gave wrong results. But when the next slice 13 of that dataset was set as the initial slice our method worked well. The results of slices 12 and 13 of dataset 9 are given in Fig. 10(a) and (b), respectively. Our method produced good results for the remaining 5 sets (10–14) except for few upper slices that are affected by partial volume effect (PVE) at the skull boundary. The result for the slice 33 of dataset 10 is shown in Fig. 10(c). Fig. 10(c) shows only strips of brain portion at the bottom left. Specialized methods are needed to deal such abnormal slices.

During our experiments we observed that the head masks produced in Stage-1 of few slices had cavities, either due to scalp tissues having low intensity values or due to wrap around artifact. Sometimes the weak boundaries of skull, due to PVE, did not produce the closed contour for the skull and affected the results in SRP or BEP. These two factors will split our brain portion into many pieces during the extraction process. But our BEM2DE picked up the regions

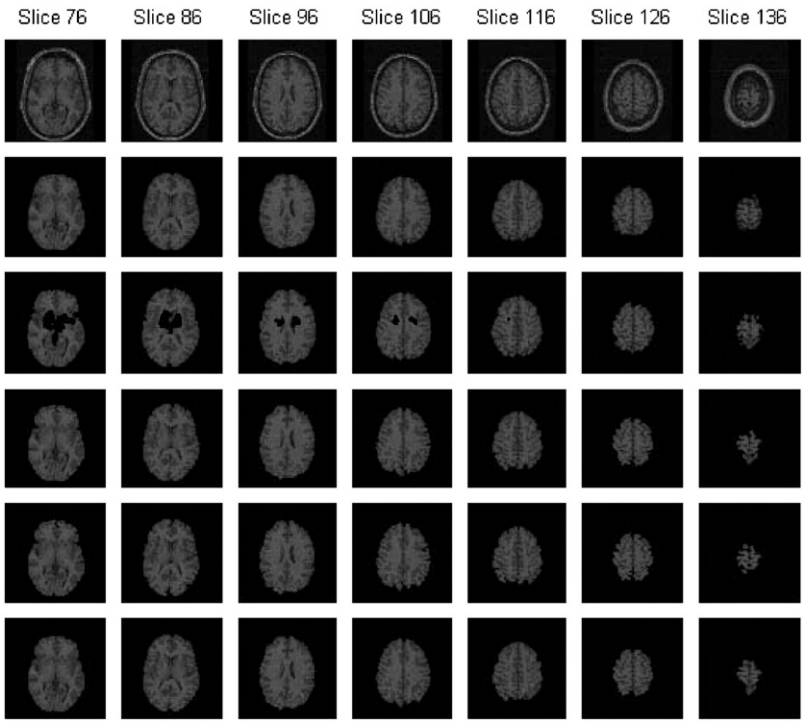

Fig. 7. Brain portion extracted using the existing and proposed algorithms on *T*1 head scans selected from the lower portions of axial volume of BEE web service. Row 1 shows original *T*1 scans and rows 2–6 show brain portion extracted by BET, BSE, BEM2D, BEM2DE and MLS, respectively.

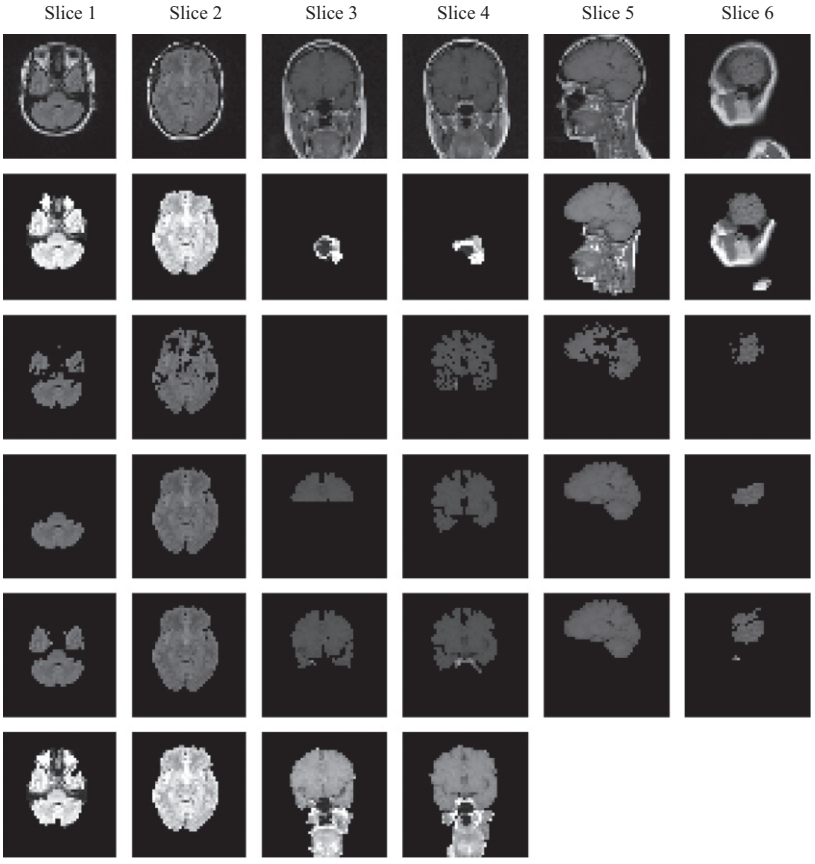

Fig. 8. Brain portion extracted using the existing and proposed algorithms on *T*1 head scans selected from real datasets. Row 1 shows original *T*1 scans and rows 2–6 show brain portion extracted by BET, BSE, BEM2D, BEM2DE and MLS, respectively.

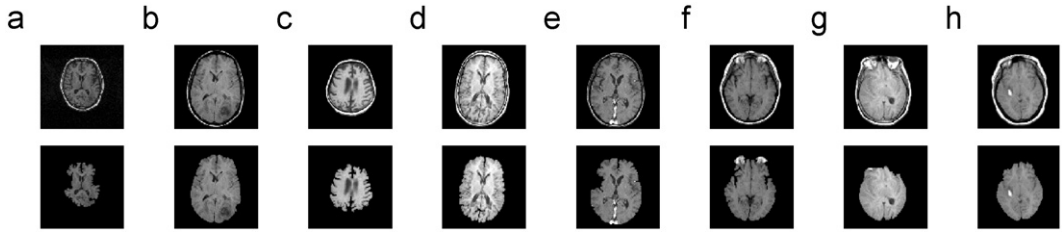

Fig. 9. Initial slices selected from datasets 1–8 of WBA are in row 1 and the respective brain portions extracted by proposed method are in row 2. (a) Slice 62 of dataset 1, (b) slice 12 of dataset 2, (c) slice 9 of dataset 3, (d) slice 12 of dataset 4, (e) slice 12 of dataset 5, (f) slice 12 of dataset 6, (g) slice 12 of dataset 7 and (h) slice 12 of dataset 8.

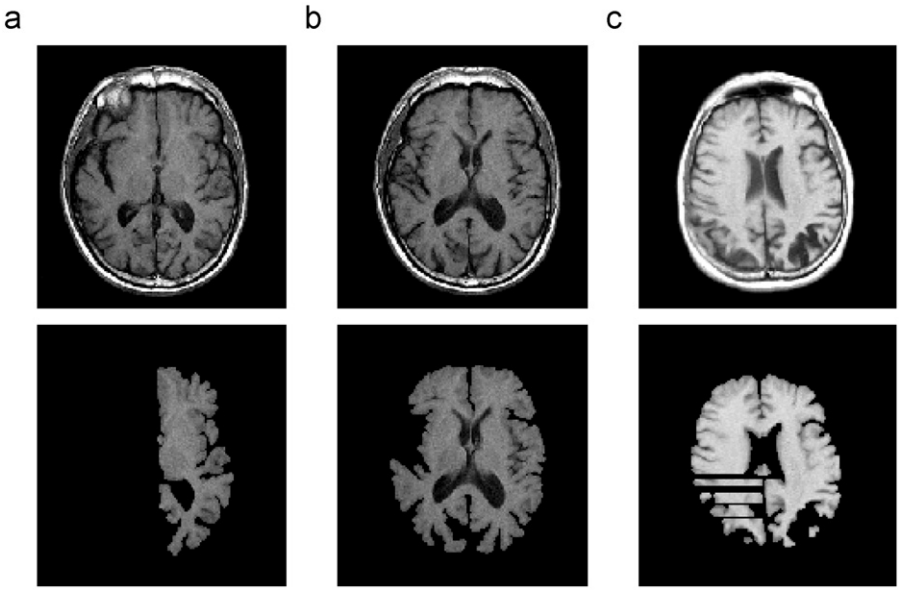

Fig. 10. Row 1 shows the originals and row 2 shows the extracted brain portions: (a) slice 12 of dataset 9, (b) slice 13 of dataset 9 and (c) slice 33 of dataset 10.

corresponding to brain in each slice and constructed brain with more than one connected region.

The extracted brain region from real datasets, BEE web service subjects and WBA datasets were visually inspected by two radiological experts and two experienced neurologists. The qualitative assessment was done by analyzing the remaining non-brain regions and the regions of brain tissues lost in the stripped brain area. The experts opined that the brain has been extracted correctly in all the images except a few that are affected by PVE and wrap around artifacts. The qualitative validation shows that the results produced by our methods are comparable to or better than the popular methods BET, BSE and MLS.

The failure of the methods BET, BSE and MLS on certain slices of MRI of head scans and success of the proposed methods may be due to the following reasons:

i. The existing methods require certain parameters as input to start the procedure. These parameters depend on image specific knowledge. Therefore, in datasets with abnormal slices, the input parameters may not fit for the abnormal slices and failed. The proposed methods are adaptive to image characteristics and hence succeeded in extracting those brain portions.
ii. The existing methods are designed for normal datasets and thus they failed for certain abnormal datasets especially for tumorous volumes. The proposed methods worked well for both normal and abnormal datasets.
iii. The existing methods are model based methods. They require the input image to have head up position and less neck portions. So they require some preprocessing technique like rotation and cropping to bring the image into the required position. But the proposed methods require only the skull-brain boundary detection and not model-based approach.
iv. The existing methods require preprocessing of the image, like bias correction and contrast enhancement. The proposed methods do not require any of these. Therefore, when raw images with artifacts, INU and low contrast are given as inputs, these methods failed while the proposed methods worked well.
v. MLS is not modeled to process sagital type image. Hence it failed for sagital orientation.

Our methods start from the mid slices and propagate up or down to process the other slices. If this initial extraction fails, then the whole process fails. Further, when PVE affects the skull boundary then the brain extraction is not good. These are the drawbacks of our methods.

5. Conclusion

In this paper we have presented two fully automatic brain extraction methods with 2-D and 3-D approaches to extract brain from *T*1 MRI of head scans. The 3-D based BEM2DE performed better than BEM2D. The proposed methods do not require any external parameter to process the MRI of head scans and thus qualify to be an automatic BEA. These methods are not model based approaches and thus are suitable for any orientation and even for low contrast images. Experimental results show that our methods worked well on

both normal and certain types of abnormal brain datasets. Our 3-D based method worked well even for abnormal datasets available in WBA where BSE, BET and MLS failed. This is purely an intensity based automatic tool and hence can be implemented as a part of any automatic brain image processing system. This method is extended to 3-D processing and is under progress.

Conflict of interest statement

None declared.

Acknowledgments

The authors wish to thank Dr. K.G. Srinivasan, MD, RD, Consultant Radiologist, Dr. Ritesh, KGS Advanced MR & CT Scan, Madurai, Tamilnadu, India, and Dr. N. Karunakaran, DMRD, DNB, Consultant—Radiodiagnosis, Meenakshi Mission Hospital and Research Center, Madurai, Tamilnadu, India, for providing the MR Head scans and for obtaining the qualitative validation. The authors would also wish to thank Dr. R. Durairaj, MD (Paed), DM (Neuro), Consultant Neurologist, Department of Neurology, Dr. K. Selvamuthukumaran MCh (Neuro), Sr. Consultant, Department of Neuro Surgery, Meenakshi Mission Hospital and Research Center, Madurai, Tamilnadu, India, Dr. S.P. Balachandran, MD, DM (Neuro), Neurologist, Dindigul Neuro Center, Dindigul District, Tamilnadu, India, and Dr. R.S. Jayasree, Scientist, Sree Chitra Tirunal Institute for Medical Science and Technology (SCTIMST), Thiruvananthapuram, Kerala, India, for their help in verifying the results. The authors wish to thank the unknown referees for their constructive suggestions, which resulted in presenting this paper in a clear and precise manner for publication.

This work is catalyzed and funded by Science for Equity, Empowerment and Development (SEED) Divisions, Department of Science and Technology (DST), Government of India, New Delhi, Grant number: SP/YO/011/2007 under the Scheme for Young Scientists and Professionals (SYSP).

References

[1] A.P. Dhawan, Medical Image Analysis, John Wiley Publications and IEEE Press, 2003.
[2] C. Fennema-Notestine, I.B. Ozyurt, C.P. Clark, S. Morris, A. Bischoff-Grethe, M.W. Bondi, T.L. Jernigan, B. Fischl, F. Segonne, D.W. Shattuck, R.M. Leahy, D.E. Rex, A.W. Toga, K.H. Zou, G.G. Brown, Quantitative evaluation of automated skull-stripping methods applied to contemporary and legacy images: effects of diagnosis, bias correction, and slice location, Human Brain Mapping 27 (2) (2006) 99–113.
[3] J. Ashburmer, K.J. Friston, Voxel based morphometry: the methods, NeuroImage 11 (2000) 805–821.
[4] S.M. Smith, Fast robust automated brain extraction, Human Brain Mapping 17 (2002) 143–155.
[5] S. Sandor, R. Leahy, Surface-based labeling of cortical anatomy using a deformable atlas, IEEE Transactions on Medical Imaging 16 (1) (1997) 41–54.
[6] D.W. Shattuck, S.R. Sandor-Leahy, K.A. Schaper, D.A. Rottenberg, R.M. Leahy, Magnetic resonance image tissue classification using a partial volume model, Neuroimage 13 (5) (2001) 856–876.
[7] B.D. Ward, Intracranial Segmentation, Biophysics Research Institute, Medical College of Wisconsin, Milwaukee, WI, 1999.
[8] H. Hahn, H.O. Peitgen, The skull stripping problem in MRI solved by a single 3D watershed transform, in: Paper Presented at the Proceedings of MICCAI, LNCS, vol. 1935, 2000, pp. 134–143.
[9] A.H. Zhuang, D.J. Valentino, A.W. Toga, Skull-stripping magnetic resonance brain images using a model-based level set, NeuroImage 32 (1) (2006) 79–92.
[10] L. Lemieux, Fast, accurate, and reproducible automatic segmentation of the brain in T1-weighted MR volumes, Magnetic Resonance in Medicine 42 (1) (1999) 127–135.
[11] S.M. Atkins, B.T. Mackiewich, Fully automatic segmentation of the brain in MRI, IEEE Transactions on Medical Imaging 17 (1) (1998) 98–107.
[12] K. Somasundaram, T. Kalaiselvi, Brain extraction method for T1 magnetic resonance scans, in: Paper Presented at the Proceedings of The International Conference on Signal Processing and Communication (IEEE-SPCOM2010), Indian Institute of Sciences (IISc), Bangalore, India, 2010, pp. 1–5.
[13] K. Somasundaram, T. Kalaiselvi, Fully automatic brain extraction algorithm for axial T2-weighted magnetic resonance images, Computers in Biology and Medicine 40 (10) (2010) 811–822.
[14] J.M. Lee, J.H. Kim, I.Y. Kim, J.S. Kwon, S.I. Kim, Evaluation of automated and semi-stripping algorithms: similarity index and segmentation error, Computers in Biology and Medicine 33 (6) (2003) 495–507.
[15] V. Grau, A.U.J. Mewes, M. Akaniz, R. Kikinis, S.K. Warfield, Improved watershed transform for medical image segmentation using prior information, IEEE Transactions on Medical Imaging 23 (4) (2004) 447–458.
[16] S.M. Hartley, A.I. Scher, E.S.C. Korf, L.R. White, L.J. Launer, Analysis and validation of automated skull stripping tools : a validation study based on 296 MR images from the Honolulu Asia aging study, Neuroimage 30 (2006) 1179–1186.
[17] K. Boesen, L. Rehm, K. Schaper, S. Stoltzner, R. Woods, E. Luders, D. Rottenberg, Quantitative comparison of four brain extraction algorithms, NeuroImage 22 (2004) 1255–1261.
[18] D.E. Rex, D.W. Shattuck, R.P. Woods, K.L. Narr, E. Luders, K. Rehm, S.E. Stolzner, D.A. Rottenberg, A.W. Toga, A meta-algorithm for brain extraction in MRI, NeuroImage 23 (2004) 625–637.
[19] F. Segonne, A.M. Dale, E. Busa, M. Glessner, D. Salat, H.K. Hahn, B. Fischl, A hybrid approach to the skull stripping problem in MRI, NeuroImage 22 (2004) 1060–1075.
[20] A. Huang, R. Abugharbieh, R. Tam, A. Traboulsee, MRI brain extraction with combined expectation and geodesic active contours, in: IEEE International Symposium on Signal Processing and Information Technology, 2006, pp. 107–111.
[21] G.M. Ravinda, N.R. Jagath, Fully automatic peeling technique for T1-weighted, high-quality MR head scans, International Journal of Image and Graphics 4 (2) (2004) 141–156.
[22] M. Sonka, V. Hlavac, R. Boyle, Image Processing, Analysis and Machine Vision, Brooks/Cole Publishing Company, 1999.
[23] P. Jaccard, The distribution of flora in the alpine zone, New Phytology 11 (2) (1912) 37–50.
[24] A.P. Zijdenbos, B.M. Dawant, R.A. Margolin, A.C. Palmer, Morphometric analysis of white matter lesions in MR images, IEEE Transactions on Medical Imaging 13 (1994) 716–724.

K. Somasundaram was born in the year 1953. He received MSc degree in Physics from the University of Madras, Chennai, India, in 1976, the Post Graduate Diploma in Computer Methods from Madurai Kamaraj University, Madurai, India, in 1989 and the PhD degree in Theoretical Physics from Indian Institute of Science, Bangalore, India, in 1984. He is presently the Professor and the Head of the Department of Computer Science and Applications, and Head, Computer Centre at Gandhigram Rural Institute, Gandhigram, India. From 1976 to 1989, he was a Professor with the Department of Physics at the same institute. He was previously a Researcher at an International Centre for Theoretical Physics, Trieste, Italy, and a Development Fellow of Commonwealth Universities at the School of Multimedia, Edith Cowan University, Australia. His research interests are in image processing, image compression and medical imaging. He is a Life member of Indian Society for Technical Education. He is also an annual member in ACM, USA and IEEE Computer Society, USA.

T. Kalaiselvi was born in Tamilnadu, India, in 1974. She received her Bachelor of Science (BSc) degree in Mathematics and Physics in 1994 and Master of Computer Applications (MCA) degree in 1997 from Avinashilingam University, Coimbatore, Tamilnadu, India. From 1997 to 1998 she was a Lecturer in Department of Computer Science, Avinahilingam University, India. Since 1998, she has been with Gandhigram Rural Institute, Dindigul, Tamilnadu, India, where she was a Lecturer in Department of Computer Science and Applications till 2006. From 2006 she was a full time research scholar in the same department and was awarded a PhD degree in February, 2010. In 2008, she received a project from Department of Science and Technology (DST), Government of India under Scheme for Young Scientist and Professional (SYSP), Science for Equity, Empowerment and Development (SEED) Division for three years (2008–2011). Now she is working as Assistant Professor in the same Department. Her research focuses on Brain Image Processing and brain tumor or lesion detection from MR Head Scans to enrich the Computer Aided Diagnostic process, Telemedicine and Tele radiology services. She is an Academic Community Member (ACM) in International Congress for Global Science and Technology (ICGST) and Life Member (LM) in Indian Society for Technical Education (ISTE).